Effects of some parameters on the divertor plasma sheath characteristics and fuel retention in castellated tungsten tile gaps*

Sang Chao-Feng(桑超峰)[a)†], Dai Shu-Yu(戴舒宇)[a)], Sun Ji-Zhong(孙继忠)[a)], Bonnin Xavier[b)], Xu Qian(徐 倩)[c)], Ding Fang(丁 芳)[c)], and Wang De-Zhen(王德真)[a)‡]

[a)] *Key Laboratory of Materials Modification by Laser, Ion and Electron Beams (Ministry of Education), School of Physics and Optoelectronic Engineering, Dalian University of Technology, Dalian* 116024, *China*
[b)] *LSPM-CNRS, Université Paris 13, Sorbonne Paris Cité, Villetaneuse* 93430, *France*
[c)] *Institute of Plasma Physics, Chinese Academy of Sciences, Hefei* 230031, *China*

(Received 1 March 2014; revised manuscript received 1 April 2013; published online 24 September 2014)

Castellation of plasma facing components is foreseen as the best solution for ensuring the lifetime of future fusion devices. However, the gaps between the resulting surface elements can increase fuel retention and complicate fuel removal issues. To know how the fuel is retained inside the gaps, the plasma sheath around the gaps needs to be understood first. In this work, a kinetic model is used to study plasma characteristics around the divertor gaps with the focus on the H^+ penetration depth inside the poloidal gaps, and a rate-theory model is coupled to simulate the hydrogen retention inside the tungsten gaps. By varying the magnetic field strength and plasma temperature, we find that the H^+ cyclotron radius has a significant effect on the penetration depth. Besides, the increase of magnetic field inclination angle can also increase the penetration depth. It is found in this work that parameters as well as the penetration depth strongly affect fuel retention in tungsten gaps.

Keywords: divertor gaps, penetration depth, plasma sheath, fuel retention

PACS: 52.40.Kh, 52.55.Rk, 52.65.Rr, 52.65.–y **DOI:** 10.1088/1674-1056/23/11/115201

1. Introduction

Castellation is thought to be the best solution to ensuring the thermo-mechanical durability and integrity of plasma facing components (PFCs) under high heat flux loads,[1,2] especially when considering the use of metals as the plasma facing material (e.g., tungsten (W) and beryllium in ITER).[3] However, issues such as material migration into gaps, and the subsequent fuel retention, are of crucial importance for fusion devices with castellated PFCs. These issues would bring great challenges for fuel removal.[3] Therefore, concerns over the plasma characteristics and fuel accumulation in the gaps call for dedicated studies.

Experimental studies[4,5] on the fuel inventory inside the PFCs in different fusion devices showed that the divertor gaps can increase fuel retention significantly. Moreover, the experimental results also indicated that fuel retention in gaps depends on the plasma parameters as they vary remarkably in different fusion devices.[6,7] Therefore, an understanding of the influence of gap parameters on fuel inventory inside the gaps is required. As is well known, fuel accumulation inside the gaps is influenced directly by the plasma behavior around gaps, so it is important to study the plasma characteristics around this region. Calculations of fuel accumulation in gaps and its subsequent release need a model to consider factors such as surface temperature and chemistry, and an adequate description of the plasma interaction with the gap sidewall. Due to the complicated geometry and steep gradients of the plasma around the gap entrance, fluid models are not suitable for studying the plasma characteristics around the gaps, and instead, a kinetic model is needed. Such kinetic descriptions can be obtained, for instance, by particle-in-cell (PIC) methods, which have been applied extensively to edge plasma studies. Recently, a number of simulations have been carried out on the divertor gap sheath region using the PIC method.[8–11] For the fuel retention investigation, various simulation methods such as density functional theory (DFT), molecular dynamics (MD), kinetic Monte Carlo (KMC)[12] and rate theory method[13] have been successfully applied. However, due to the limitation of length and time scales, most models are not suitable for the fuel inventory on a macroscopic scale except the rate theory method.

In this work, a two-dimensional (2D) in space and three-dimensional (3D) in velocity (2D3V) edge plasma particle-in-cell (EPPIC2D) code[14] is used to study the plasma characteristics around the gaps of divertor tiles under different operation parameters, and the 2D hydrogen isotope inventory processes code (HIIPC)[15] based on the rate theory is employed, with

*Project supported by the National Magnetic Confinement Fusion Science Program, China (Grant No. 2013GB109001), the National Natural Science Foundation of China (Grant Nos. 11275042 and 11305026), and the Fundamental Research Funds for the Central Universities of Ministry of Education of China (Grant No. DUT14RC(3)039).

†Corresponding author. E-mail: sang@dlut.edu.cn
‡Corresponding author. E-mail: wangdez@dlut.edu.cn

© 2014 Chinese Physical Society and IOP Publishing Ltd

the input supplied by EPPIC2D, to study the effect of these parameters on the hydrogen isotope retention inside the W tiles. Through this study, the relationship between penetration depth and cyclotron radius of the ions is established, and the effects of plasma parameters and magnetic field on the penetration depth as well as fuel retention are analyzed and discussed.

2. Simulation models

In this work, the 2d3v PIC code EPPIC2D is employed to study the plasma characteristics in the gap region of a castellated divertor. The technique is based on the electrostatic PIC model, similar to the model in Refs. [16]–[18], and the code has been successfully used to study hydrocarbons deposited inside the gaps.[19] During the simulation, the trajectories of charged particles are tracked by solution of Newton's equations of motion, where the electric field is obtained by solving Poisson's equation. The electric potential, plasma density distribution, particle and energy fluxes to the wall, which are the basic information for studying plasma material interactions, could be obtained.

We define the gap along the poloidal direction as a poloidal gap. Figure 1 shows the schematic of the simulation domain representing a cross section of a poloidal gap: z represents the gap depth direction, and x denotes the toroidal direction. The other axis (not shown in the schematic) is aligned along the poloidal direction. The bulk plasma and the gap bottom plane serve as the top and bottom boundaries, respectively. Periodic boundary conditions are used for left and right boundaries. The charged particles are injected from the top boundary, which are treated as an ideal plasma source, with Bohm velocity ($C_s = \sqrt{k_b(T_e + T_i)/m_i}$, where k_b is the Boltzmann's constant; T_e and T_i are the electron and ion plasma temperature, respectively; m_i is the mass of the ion) along the magnetic field direction and Maxwellian velocity distributions in the perpendicular direction. The electric potential is fixed at zero for the top boundary and $V_0 = -3kT_e$ at the bottom boundary and material surfaces,[20] where V_0 is the floating potential. The uniform magnetic field makes an inclination angle α with respect to the plasma facing surface (PFS). In the simulation, the traced particles are H^+ and electrons. The simulation domain is represented by 256×256 cells (200 particles per cell) during the overall simulation, in which the cell size is kept to be smaller than the Debye length. For the convenience of presentation, the tile surfaces are marked in sequence as Side 1, Side 2, Side 3, and Side 4, as shown in Fig. 1. In this work, the divertor plasma is assumed to be fully ionized, and collisions between charged particles and neutrals are neglected. The Coulomb collisions between charged particles e–e, e–H^+, and H^+–H^+) are included in our model since they are very important for such high-density low-pressure plasmas. The code runs until the simulated plasma reaches a steady state.

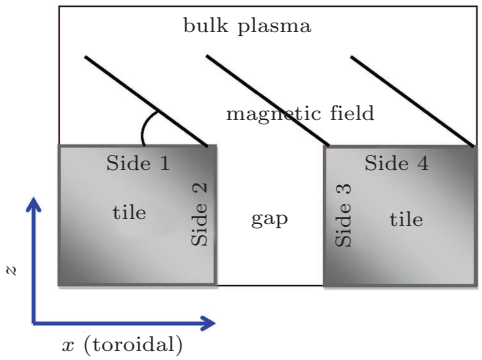


Fig. 1. (color online) Schematic diagram of the simulation domain, which is taken as being two-dimensional in space.

In order to model the fuel retention inside the W tiles, a 2D rate theory based code HIIPC2D[15] is used, to be coupled with EPPIC2D. For W materials, during hydrogen flux implantation, hydrogen atoms (only hydrogen atoms exist inside the material) will diffuse toward the place where the solute hydrogen concentration is lower. In the course of this diffusion, most atoms will be trapped by the trap sites. The retention process can be represented by a set of reaction-diffusion equations[21]

$$\frac{\partial C_s(x,z,t)}{\partial t} = \frac{\partial}{\partial x}\left(D\frac{\partial C_s(x,z,t)}{\partial x}\right) + \frac{\partial}{\partial z}\left(D\frac{\partial C_s(x,z,t)}{\partial z}\right) + \Gamma_0\phi(x,z) - \sum_{i=1}^{n}\frac{\partial C_{t,i}(x,z,t)}{\partial t}, \quad (1)$$

$$\frac{\partial C_{t,i}(x,z,t)}{\partial t} = \frac{2Da_0}{3}\left(C_s\left(C_{t,i}^0 - C_{t,i}\right) - \frac{12C_{t,i}}{a_0^3}\exp\left(-\frac{E_{i,\mathrm{dtrap}}}{k_bT}\right)\right), \quad (2)$$

where C_s is the solute hydrogen concentration, $C_{t,i}$ is the trapped hydrogen concentration in trap type i, D is the diffusion rate coefficient expressed using an Arrhenius–Boltzmann relation $D = D_0\exp(-E_m/k_bT)$,[22] D_0 is the diffusion constant, E_m is the energy barrier, Γ_0 is the incident hydrogen flux, $\phi(x,z)$ is the hydrogen implantation profile, a_0 is the lattice constant, $C_{t,i}^0$ is the initial concentration of the i-th trap site, $E_{i,\mathrm{dtrap}}$ is the binding energy of hydrogen within a trap of type i, and T is the temperature of the material.

During the diffusion process, some of the atoms will reach the PFS or back surface of the W wall. Then, the surface recombination process occurs, by which two solute hydrogen atoms combine into a molecule and are released. It can be expressed as[22]

$$J_s = K_rC_s^2, \quad (3)$$

where K_r is the recombination rate coefficient, which is determined by[23]

$$K_r = K_{r0}\exp(-E_r/kT). \quad (4)$$

In the coupled model, the particle fluxes to each side of the tiles are used as input parameters for the model of HIIPC2D.

3. Results and discussion

In this work, unless otherwise stated, the simulation parameters are taken as follows: plasma density $n_e = n_i = 1.0 \times 10^{19}$ m^{-3}, plasma temperature $T_e = T_i = 20$ eV, simulation domain 2.4 mm×2.4 mm with a gap of 0.6 mm in width (y-direction) and 0.9 mm in depth (z-direction), uniform magnetic field with strength $B = 2$ T and inclination angle $\alpha = 2^\circ$ with the PFS (see Fig. 1). These parameters are similar to those of the EAST tokamak, which is upgrading its upper divertor to W and the researchers will focus on the investigation of fuel retention in the W gaps.[24] Although the fuel retention is not a very crucial problem for EAST because no tritium is used, the present work focuses on finding the parameter dependence of fuel retention inside the W divertor tiles. The parameters for the fuel retention inside the W in Eqs. (1)–(4) are taken to be the same values as used in Ref. [13].

3.1. Effect of magnetic field strength

First, we consider the plasma in the gap region. There are almost no electrons inside the gaps, whereas the H can penetrate into the gap.[14] The electrons are totally confined by the magnetic field due to their small radius (the electron cyclotron radius is about 7.5×10^{-3} mm). The cyclotron radius of H^+, about 0.3 mm, is of the same scale as the gap width (0.6 mm), which increases the chance of an H^+ penetrating into the gap through its cyclotron motion. The separation between electron and ion at the entrance of the gaps creates a virtual anode, i.e., a potential hill, which can suppress the H^+ penetrating deeper inside the gaps.[18] Different fusion devices have findings similar but different in detail,[25,26] and this influences the fuel inventory in the gap sidewall. Therefore, it is quite important to understand the influences of different parameters on the plasma characteristics of divertor gaps as well as the fuel retention in the tiles.[27,28]

To better understand how H^+ species penetrate into the gaps, we first vary B under otherwise identical conditions. Figure 2 shows the H^+ flux distributions on each side of the tiles during the steady-state at different B values: (a) 1 T, (b) 2 T, (c) 3 T, (d) 4 T. The flux to Side 3 of the tiles, which faces the plasma flux in the gap, shows a complex decay structure. The fluxes to the corner region of Side 3 and Side 4 increase with B increasing due to the good confinement, i.e., the stronger magnetic field makes the ions move along with it better, resulting in the incident flux focusing more on the corners of Side 3 and Side 4. Although Side 2 is in the plasma shadow, ion fluxes to Side 2 can still be observed at different values of B, which is in agreement with the simulation results of Komm *et al.*[18] The particle fluxes to the gap side (Sides 2 and 3) show a strong asymmetry, both in the strength and in the depth. Since the flux strength and depth to Side 3 are larger than to Side 2, we define the depth of flux to Side 3 (decay length as 0.1% of the normalization strength) as the penetration depth in this work. It can be seen that for $B = 1$ T, the H^+ species can penetrate into the gaps over 0.9-mm deep (in our study, the simulated domain covers a gap depth of 0.9 mm). When B increases up to 2 T, the penetration depth decreases down to 0.6 mm. When

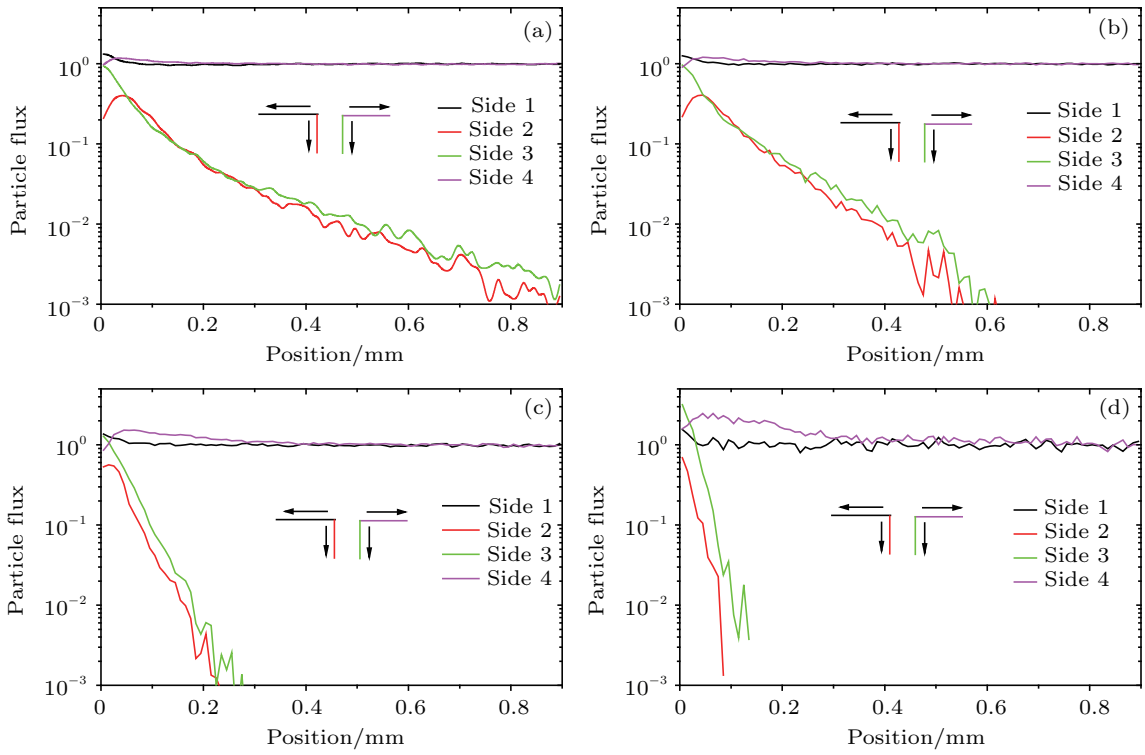


Fig. 2. (color online) Particle fluxes to each side of the tiles, obtained from EPPIC2D at magnetic field strengths of (a) 1 T, (b) 2 T, (c) 3 T, and (d) 4 T, in a steady state. The corner of each tile serves as its position origin. The flux is normalized to the averaged flux to the top sides (Side 1 and Side 4) away from the corners.

B further increases, it is found that the penetration depth decreases continuously until the H^+ species hardly penetrates into the gaps. Further analysis shows that the cyclotron radius of H^+ is important in determining the extent to which the H^+ species penetrate into the gaps. Only when the cyclotron radius of H^+ is larger than the gap width will the penetration length of H^+ into the gaps be noteworthy. As B increases and the cyclotron radius of H^+ decreases, the penetration depth is shortened, which can be seen in Fig. 2.

We are most interested in the fuel retention in the gap region of the W tiles. The plasma fluxes provided by EPPIC2D shown in Fig. 2 are taken as input parameters for HIIPC2D to monitor the fuel inventory distributions near and inside the gaps. The effect of the magnetic field strength on the hydrogen isotope retention inside the gap sidewall of W material is thus studied. Figure 3 shows the hydrogen isotope retention distributions for different values of B: (a) 1 T, (b) 2 T, (c) 3 T, (d) 4 T, after 20-s plasma exposure and 50-s outgassing. We can see that the hydrogen retained in the sidewall decreases with the magnetic field strength B increasing, because of the reduction of the H^+ penetration depth (see Fig. 2). In addition, the retention distribution asymmetry in the sidewall (Sides 2 and 3) becomes evident with B increasing. Figure 4 shows the time evolutions of the fuel inventory in the sidewall during and after plasma exposure for different values of B. In the first 20 s ("pulse on" time), the fuel inventory increases with time going by, and then decreases during the outgassing period due to the desorption of the hydrogen isotopes.[13] At the time $t = 70$ s, the retention quantity in the sidewall falls from 2.3×10^{17} atoms to 1.9×10^{16} atoms when the magnetic field B increases from 1 T to 4 T, indicating that increasing B can reduce the quantity of retained hydrogen isotopes dramatically.

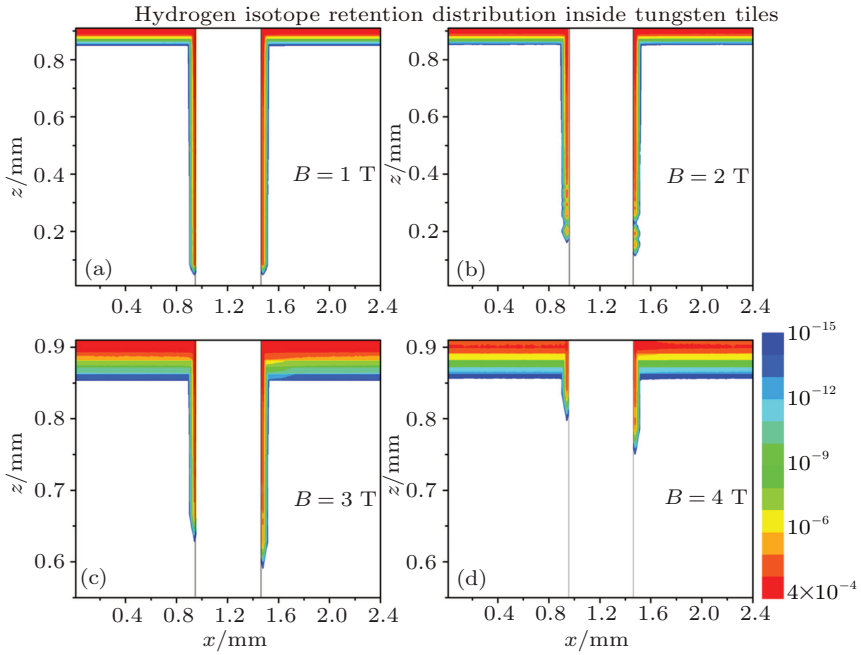


Fig. 3. (color online) Hydrogen isotope retention distributions inside W tiles after 20-s plasma exposure followed by 50-s outgassing, at different magnetic field strengths of (a) 1 T, (b) 2 T, (c) 3 T, and (d) 4 T in a steady state.

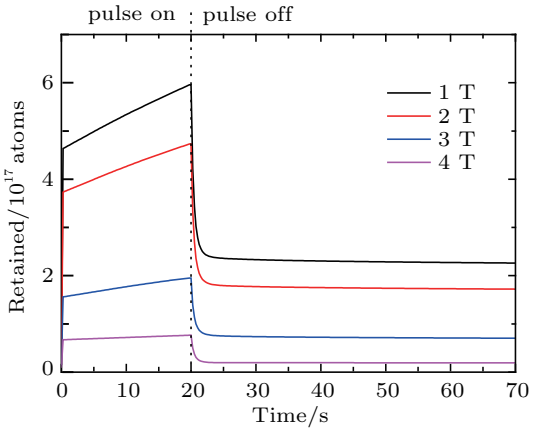


Fig. 4. (color online) Hydrogen isotope retention quantity evolutions inside the W sidewall at different magnetic field strengths during 20-s plasma exposure followed by 50-s outgassing.

3.2. Effect of plasma temperature

Since the penetration depth of H^+ inside the gaps can influence the fuel inventory in the gap sidewall, we focus on the fuel retention as well as penetration depth of H^+ inside the gaps in this work. In a tokamak, various operation modes or different shots have different divertor plasma parameters. To study the plasma sheath and fuel retention under these conditions, for different cases, simulation is necessary. H^+ fluxes to each side of the tiles obtained from EPPIC2D at different plasma temperatures 5 eV, 10 eV, 20 eV, and 30 eV, for steady-state operation, are shown in Figs. 5(a)–5(d). It can be seen that the penetration depth increases with the plasma temperature rising. The cyclotron radius of a charged particle in the magnetic field can be expressed as $r_c = mv_\perp/qB$, where B is

the magnetic field strength, m, $v_\perp$, q are the mass, velocity component perpendicular to the magnetic field, and charge of the particle, respectively. Since the velocity is proportional to $T^{0.5}$ (T is the plasma temperature), we can obtain $r_c \propto T^{0.5}$, i.e., the cyclotron radius of a charged particle increases with the plasma temperature rising. Therefore, it can be used to explain why the penetration depth of H^+ increases with the plasma temperature rising. Besides, the flux asymmetry with respect to the sidewall is also observed during plasma temperature variation. Under very high plasma temperature circumstances, it can be predicted from this conclusion that the penetration depth of hydrogen cations will be much larger than during steady-state operation.[25] It can also be deduced from this finding that for scenarios operating with divertor detachment, in which the divertor plasma temperature is extremely low,[30] the H^+ can barely penetrate into the poloidal gaps. However, due to the existence of the impurities in the divertor region during detachment, the fuel retention process becomes much more complicated, which is out of the focus of this work.

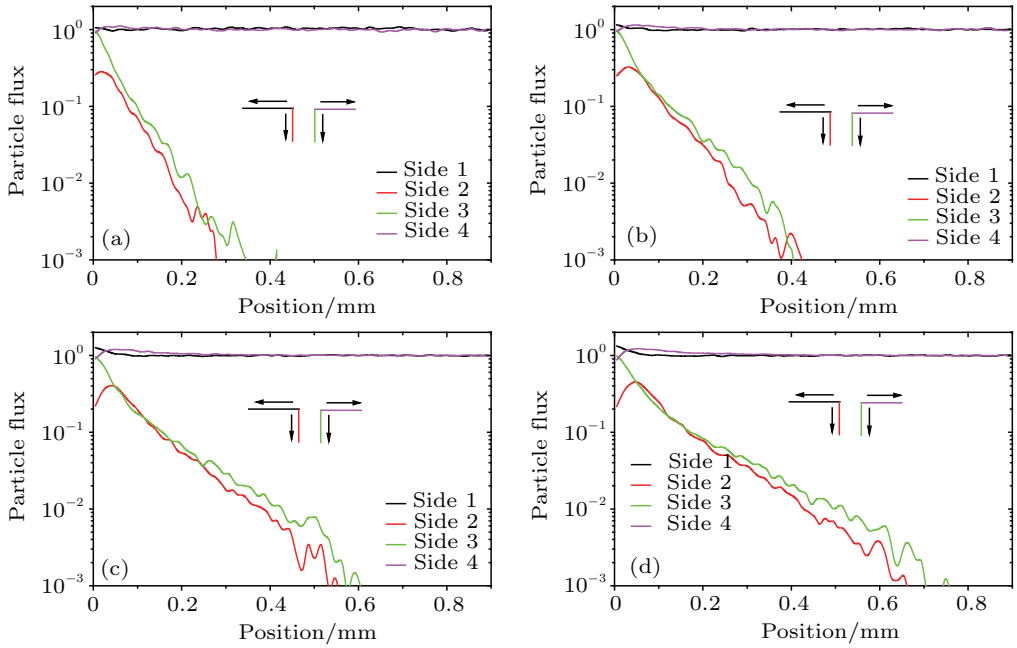


Fig. 5. (color online) Particle fluxes to each side of the tiles, obtained from EPPIC2D at different plasma temperatures of (a) 5 eV, (b) 10 eV, (c) 20 eV, and (d) 30 eV in a steady state. The flux is normalized to the averaged flux to the top sides (Sides 1 and 4) away from the corners.

The effect of the plasma temperature on the fuel retention in the sidewall is also studied. Figure 6 presents the fuel inventory evolutions at different plasma temperatures. It shows that the fuel retention quantity increases with the plasma temperature rising obviously. Two reasons can explain the increase. The first reason is the penetration depth: it is shown in Fig. 5 that a higher plasma temperature could lead to a larger penetration depth, thus increasing the fuel inventory in the sidewall. The other reason is the flux strength: a higher plasma temperature can lead to a larger flux. In the simulation, the normalizing factors (i.e., the averaged flux to the top side) are 4.1×10^{22} ions·m^{-2}·s^{-1} (5 eV), 6.5×10^{22} ions·m^{-2}·s^{-1} (10 eV), 1.09×10^{23} ions·m^{-2}·s^{-1} (20 eV), and 1.40×10^{23} ions·m^{-2}·s^{-1} (30 eV), respectively. Since the fuel inventory does not proportionally increase with incident flux increasing,[31] the trend that the retention quantity varies with incident flux is different from the trend that the normalization factor varies incident flux.

The penetration depth of H^+ inside the gaps is influenced by the magnetic field strength and the plasma temperature, which are both related to the cyclotron radius of H^+,

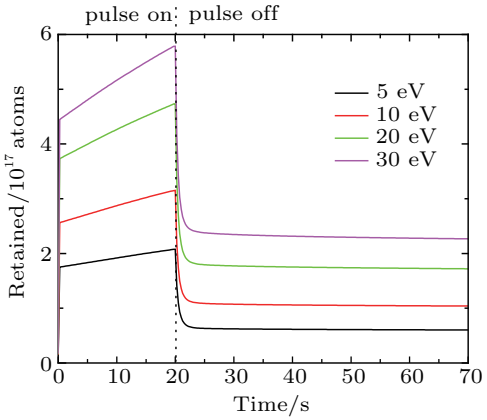


Fig. 6. (color online) Hydrogen isotope inventory evolutions inside the W sidewall at different plasma temperatures during 20-s plasma exposure followed by 50-s outgassing.

as mentioned above (shown in Figs. 2 and 5). Figure 7 displays the penetration depths versus H^+ cyclotron radius obtained from different values of B and T, respectively. We can see that the penetration depth increases with the H^+ cyclotron radius increasing, from the viewpoints of both magnetic field strength ($\propto B^{-1}$) and plasma temperature ($\propto T^{0.5}$)

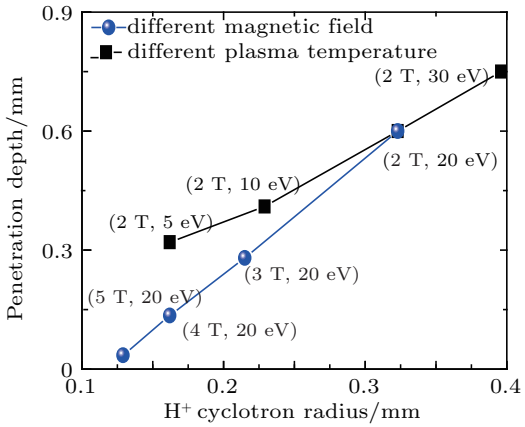


Fig. 7. (color online) H^+ penetration depths inside the gaps versus H^+ cyclotron radius for different magnetic field strengths and different plasma temperatures.

and approximates $2r_c$ on the whole. However, the penetration depth obtained from different B (blue) gradually diverges from $2r_c$ as B increases. This can be explained by the fact that a strong magnetic field can confine the charged particle well and make them run along the magnetic field, causing the penetration depth to approximate to the gap width$\times\tan(\alpha)$ (~ 0.021 mm, much smaller than the H^+ cyclotron radius). Therefore, the penetration depth is smaller than $2r_c$ as the magnetic strength increases. It is also found that the potential hill increases with plasma temperature rising, and thus restrains the penetration depth of H^+ making the ratio smaller than expected, which is similar to the results given by Komm *et al.*[18]

3.3. Effect of magnetic field inclination angle

The effect of the magnetic field angle α is studied in this section. Figure 8 shows the H^+ fluxes to each side of the tiles for different values of α: (a) 5°, (b) 10°, and (c) 15°. Because the cyclotron radius of H^+ has a large effect on the penetration depth, we select a large magnetic field strength ($B = 5$ T) to eliminate its effect. From the figure, we can see that the penetration depth of H^+ inside a gap increases with α rising and almost all of the H^+ in the gaps impinge on Side 3 as a result of good confinement, which is in agreement with the results in Refs. [32] and [33]. It is shown that H^+ can go more deeply into the gaps for larger α, which is consistent with the theoretical predictions, i.e., the plasma wetted region on Side 3 can be expressed as gap width$\times\tan(\alpha)$. The H^+ penetration depth as a function of α, obtained from simulation and theoretical analysis, are shown in Fig. 9 respectively, which shows a good consistence with the theoretical analyzes.

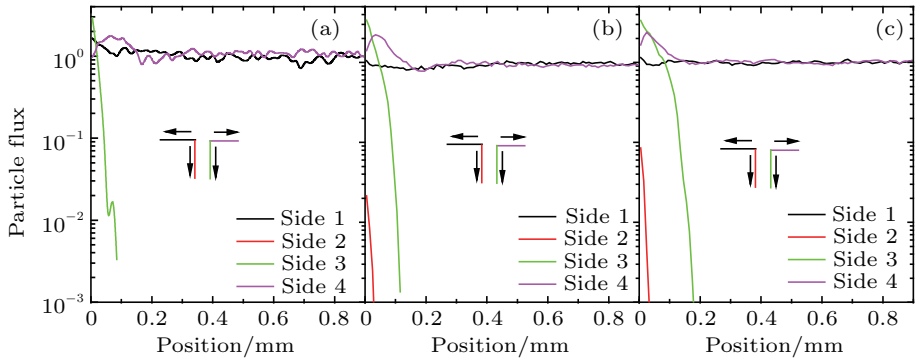


Fig. 8. (color online) Particle fluxes to each side of the tiles, obtained from EPPIC2D at different magnetic field angles of (a) 5°, (b) 10°, and (c) 15° in a steady state. The magnetic field strength is 5 T. The flux is normalized to the averaged flux to the top sides (Sides 1 and 4) away from the corners.

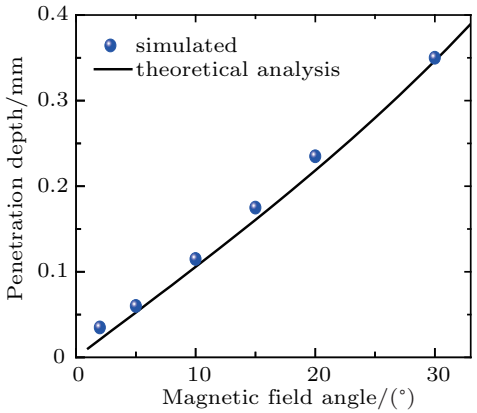


Fig. 9. (color online) H^+ penetration depth inside the gaps as a function of magnetic field angle in a steady state.

Smaller magnetic field inclination angle α has two effects: reducing the heat flux load to the PFS of the tile (Sides 1 and 4)[34,35] and reducing the penetration depth of H^+. Therefore, the fuel inventory in the sidewall of a poloidal gap increases with the magnetic field angle increasing, as shown in Fig. 10. At the end of the plasma exposure $t = 20$ s, the fuel inventories are 2.85×10^{16} atoms (2°), and 3.99×10^{16} atoms (5°), 7.37×10^{16} atoms (10°), and 1.12×10^{17} atoms (15°), respectively, which is approximately proportional to $\tan(\alpha)$. After 50-s outgassing, the retained quantities become 3.9×10^{15} atoms, 1.1×10^{16} atoms, 4.1×10^{16} atoms, and 7.14×10^{16} atoms.

From this study, it can be obtained that the penetration depth of hydrogen cations can greatly influence the fuel retention in the W gaps. Both the larger magnitude of the strength and the smaller inclination angle of the magnetic field are favorable for reducing the quantity of H^+ penetrating into the

poloidal gaps and thus the fuel inventory. Since a lower plasma temperature can reduce the heat flux on the PFS and the H^+ fuel inventory in the sidewall, one should aim to diminish the plasma temperature. In addition, our simulation shows that T penetrates more deeply into a fixed-width gap when considering the H/D/T isotopic effects, which further complicates its removal and leads to fuel depletion over long pulses. The simultaneous use of D/T on the T retention is under development and not presented in the present paper.

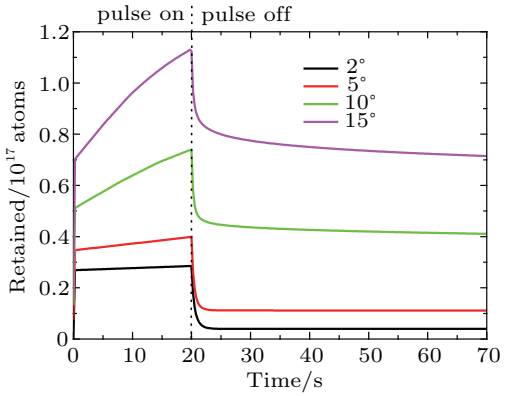


Fig. 10. (color online) Hydrogen isotope retention quantity evolutions inside the W sidewall at different values of magnetic field angle α during 20-s plasma exposure followed by 50-s outgassing.

4. Conclusions

In this work, a kinetic model is used to study the dependence of the H penetration depth inside the poloidal gaps of plasma-facing components on operation parameters. It is found that the penetration depth of H^+ decreases with the magnetic field strength (B) increasing, and increases with the plasma temperature (T) rising. The penetration depth of H^+ is about twice the cyclotron radius ($\sim 2r_c$). The penetration depth also increases with magnetic field inclination angle (α) increasing under the condition that H^+ is well confined. Effects of the magnetic field strength and angle and plasma temperature on the fuel inventory in the W gap sidewall are studied. The simulation results show the fuel inventory decreases with magnetic field strength B increasing but it increases with the magnetic field incident angle α mainly due to the variation of penetration depth, and increases with plasma temperature rising because both the penetration depth and magnitude of the incident particle flux increase. Therefore, it can be concluded that the increasing H^+ penetration depth can greatly increase the fuel retention in the gap sidewall. Further studies will involve the D–T plasma simulation as well as the T retention inside the W tiles by taking into account the isotopic effect on the retention.

References

[1] Du H L, Sang C F, Wang L, Sun J Z, Liu S C, Wang H Q, Zhang L, Guo H Y and Wang D Z 2013 *Acta Phys. Sin.* **62** 245206 (in Chinese)

[2] Huang Y, Sun J Z, Sang C F, Ding F and Wang D Z 2014 *Acta Phys. Sin.* **63** 035204 (in Chinese)

[3] Rubel M J, Coad J P and Pitts R A 2007 *J. Nucl. Mater.* **367–370** 1432

[4] Péourié B, Panayotis S, Languille P, Martin C, Dittmar T, Gauthier E, Hatchressian J C, Pascal J Y, Roubin P, Ruffe R, Tsitrone E, Vartanian S, Wang H, Beauté A, Bouvet J, Brosset C, Bucalossi J, Cabié M, Caprin E, Courtois X, Dachicourt R, Delchambre E, Dominici C, Douai D, Ekedahl A, Gunn J P, Hakola A, Jacob W, Khodja H, Likonen J, Linez F, Litnovsky A, Marandet Y, Markelj S, Martinez A, Mayer M, Meyer O, Monier-Garbet P, Moreau P, Negrier V, Oddon P, Pardanaud C, Pasquet B, Pelicon P, Petersson P, Philipps V, Possnert G, Reiter D, Roth J, Roure I, Rubel M, Saint-Laurent F, Samaille F and Vavpeti P 2013 *J. Nucl. Mater.* **438** S120

[5] Rubel M J, Sergienko G, Kreter A, Pospieszczyk A, Psoda M and Wessel E 2008 *Fusion Eng. Des.* **83** 1049

[6] Litnovsky A, Wienhold P, Philipps V, Krieger K, Kirschner A, Matveev D, Borodin D, Sergienko G, Schmitz O, Kreter A, Samm U, Richter S and Breuer U 2009 *J. Nucl. Mater.* **390–391** 556

[7] Skinner C H, Gentile C A, Hosea J C, Mueller D, Coad J P, Federici G and Haange R 1999 *Nucl. Fusion* **39** 271

[8] Dejarnac R, Komm M, Stöckel J and Panek R 2008 *J. Nucl. Mater.* **382** 31

[9] Inai K, Ohya K, Tomita Y, Kirschner A, Litnovsky A and Tanabe T 2009 *J. Nucl. Mater.* **390–391** 119

[10] Matveev D, Kirschner A, Litnovsky A, Komm M, Borodin D, Philipps V and van Oost G 2010 *Plasma Phys. Control. Fusion* **52** 075007

[11] Komm M, Dejarnac R, Gunn J P and Pekarek Z 2013 *Plasma Phys. Control. Fusion* **55** 025006

[12] Zinkle S J 2005 *Phys. Plasmas* **12** 058101

[13] Sang C, Bonnin X, Warrier M, Rai A, Schneider R, Sun J and Wang D 2012 *Nucl. Fusion* **52** 043003

[14] Sang C, Sun J and Wang D 2011 *J. Nucl. Mater.* **415** S204

[15] Sang C, Sun J, Bonnin X, Guo H and Wang D 2013 *J. Nucl. Mater.* **438** S1129

[16] Tskhakaya D, Eliasson B, Shukla P K and Kuhn S 2004 *Phys. Plasmas* **11** 3945

[17] Sang C, Sun J and Wang D 2010 *Plasma Phys. Control. Fusion* **52** 042001

[18] Komm M, Dejarnac R, Gunn J P, Kirschner A, Litnovsky A, Matveev D and Pekarek Z 2011 *Plasma Phys. Control. Fusion* **53** 115004

[19] Dai S, Sang C, Liu S, Sun J and Wang D 2012 *Fusion Eng. Des.* **87** 782

[20] Tskhakaya D, Matyash K, Schneider R and Taccogna F 2007 *Contrib. Plasma Phys.* **47** 563

[21] Ogorodnikova O, Roth J and Mayer M 2003 *J. Nucl. Mater.* **313–316** 469

[22] Frauenfelder R 1969 *J. Vac. Sci. Technol.* **6** 388

[23] Causey R 2002 *J. Nucl. Mater.* **300** 91

[24] Ding F, Luo G N, Pitts R A, Litnovsky A, Gong X Z, Ding R, Wampler W R, Stangeby P C, Carpentier S, Hellwig M, Ashikawa N, Fukumoto M, Katayama K, Chen J L, Zhou H S, Yan R, Wu J, Mao H M, Wang W Z, Xie C Y, Zuo G Z, Hu J S, Liu S L and Huang H 2014 *J. Nucl. Mater.* In Press

[25] Dejarnac R, Komm M, Gunn J P and Panek R 2009 *J. Nucl. Mater.* **390–391** 818

[26] Inai K and Ohya K 2008 *Contrib. Plasma Phys.* **48** 275

[27] Litnovsky A, Philipps V, Kirschner A, Wienhold P, Sergienko G, Kreter A, Samm U, Schmitz O, Krieger K, Karduck P, Blome M, Emmoth B, Rubel M, Breuer U and Scholl A 2007 *J. Nucl. Mater.* **367–370** 1481

[28] Wittlich K, Hirai T, Compan J, Klimov N, Linke J, Loarte A, Merola M, Pintsuk G, Podkovyrov V, Singheiser L and Zhitlukhin A 2009 *Fusion Eng. Des.* **84** 1982

[29] Zohm H 1996 *Plasma Phys. Control. Fusion* **38** 105

[30] Federici G, Skinner C H, Brooks J N, Coad J P, Grisolia C, Haasz A A, Hassanein A, Philipps V, Pitcher C S, Roth J, Wampler W R and Whyte D G 2001 *Nucl. Fusion* **41** 1967

[31] Sang C, Sun J, Bonnin X, Wang L, Du H, Huang Y and Wang D 2014 *Fusion Eng. Des.* **89** 2214

[32] Tanabe T, Sugiyama K, Skinner C H, Bekris N, Gentile C A and Coad J P 2005 *Fusion Sci. Technol.* **48** 577

[33] Inai K, Tomita Y, Kawamura G and Ohya K 2010 *Fusion Eng. Des.* **85** 1416

[34] Stangeby P C 2000 *The Plasma Boundary of Magnetic Fusion Devices*

[35] Sang C, Sun J and Wang D 2010 *Fusion Eng. Des.* **85** 1941